

Quantifying Stabilized Phase Purity in Formamidinium-Based Multiple-Cation Hybrid Perovskites

Lena Merten, Alexander Hinderhofer,* Thomas Baumeler, Neha Arora, Jan Hagenlocher, Shaik Mohammed Zakeeruddin, M. Ibrahim Dar,* Michael Grätzel, and Frank Schreiber



Cite This: *Chem. Mater.* 2021, 33, 2769–2776



Read Online

ACCESS |



Metrics & More

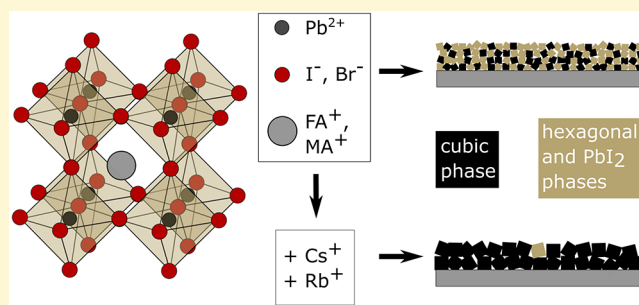


Article Recommendations



Supporting Information

ABSTRACT: A promising approach for the production of highly efficient and stable hybrid perovskite solar cells is employing mixed-ion materials. Remarkable performances have been reached by materials comprising a stabilized mixture of methylammonium (MA^+) and formamidinium (FA^+) as a monovalent cation. We compare and quantify the methods of stabilizing FA-based perovskites involving the additional blending of the smaller inorganic cations cesium (Cs^+) and rubidium (Rb^+), which can lead to an improvement in phase purity of black cubic perovskite modification. Even under excess lead iodide conditions, the presence of a separate PbI_2 phase as well as hexagonal phases, which are very common for formamidinium-containing perovskites, can be drastically reduced or even completely prevented. In this aspect, adding both Cs^+ and Rb^+ showed greater effectivity than only adding Cs^+ , enabling an increase in the percentage of the cubic phase within the material from 45% in the double-cation FA:MA mixture to 97.8% in the quadruple composition. The impact of admixing inorganic cations on the perovskite crystal structure resulted in enlarged homogeneous crystallite sizes and a less pronounced orientational order and indicated also minor modifications of unit cell sizes. Finally, we discuss the impact of the phase purity on charge-carrier recombination dynamics and solar cell performance.



INTRODUCTION

During the last decade, huge efforts were expended in the material class of hybrid organic–inorganic perovskites by the solar cell community, leading to a substantial rise in photovoltaic efficiency and a promising perspective for relatively cheap and easy to manufacture perovskite materials for solar energy.¹ For optimization of solar cell devices, material composition and structure are of crucial importance. Indeed, the composition of organic–inorganic hybrid perovskites is variable to a large extent, providing means and need for structural optimization, which in turn has a great impact on performance improvement.

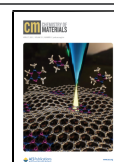
In hybrid lead halide materials APbX_3 , where X is iodide, bromide, or chloride anions, different kinds and mixtures of A cations have been investigated. The most commonly used organic molecular cation is methylammonium (MA^+), which is able to form a lead halide perovskite structure at room temperature.² In particular, the MAPbI_3 material has been widely explored due to its relatively small band gap that allows absorption of visible light.³ An even narrower band gap, which facilitates a greater amount of harvested solar energy, is exhibited by hybrid perovskites based on the formamidinium (FA^+) cation.^{4,5} In addition, FA^+ is supposed to be more thermally stable⁴ than the MA^+ cation and has the potential of outperforming the insufficient environmental^{6–8} and opera-

tional⁹ stability of MAPbI_3 , which is a major drawback for hybrid perovskite solar cells. Unfortunately, the FAPbI_3 system at room temperature exhibits a large proportion of non-photoactive (“yellow”) hexagonal δ -phase.^{5,10,11} For optical applications such as solar cells, a high phase purity of the optically active cubic (“black”) perovskite modification would be desirable. In order to exploit the excellent light harvesting and enhanced stability of the FA^+ cation, efforts have been made to stabilize the cubic phase of FAPbI_3 at room temperature.¹² This can be achieved, for example, by blending the precursors FAI and MABr ,^{13–15} which yield a mixed ion perovskite upon reaction with PbI_2 . Addition of Cs^+ to the mixture has proven to reduce the occurrence of the δ -phase even further^{16–21} and to positively affect the crystallization process.^{16,17,22,23} Also, an excess of PbI_2 has been shown to assist the suppression of the δ -phase and even benefits device performance.²⁴ However, the presence of a segregated PbI_2 phase might negatively affect charge carrier lifetimes²⁵ and

Received: October 27, 2020

Revised: March 29, 2021

Published: April 16, 2021



long-term environmental stability of the material.²⁶ This has been addressed by the addition of Rb^+ , which has proven beneficial in stabilizing the cubic FAPbI_3 phase^{10,27–31} and reducing residual PbI_2 ^{10,28} by reacting with the excess material, and has also been explored in quadruple-cation compositions of FA^+ , MA^+ , Cs^+ , and Rb^+ .^{21,23,27,32–35}

In this paper, a quantitative comparison of the structural properties of hybrid lead halide perovskites containing different cation compositions is made. In particular, the effects of including the inorganic cations Cs^+ and Rb^+ into an optimized mixture¹³ of organic cations FA^+ and MA^+ under excess lead iodide conditions were examined with regard to the occurrence of different crystal phases. For that purpose, four compositionally differing samples were prepared: the parent compound, produced from a mixture of 83% FAPbI_3 and 17% MAPbBr_3 , a similar composition with the addition of excess PbI_2 , a triple mixture of FA^+ , MA^+ , and Cs^+ cations, and the quadruple composition of FA^+ , MA^+ , Cs^+ , and Rb^+ . Although a considerable amount of research on multiple-cation perovskites has been conducted by now, this report is to the best of our knowledge the first to provide quantitative data comparing the effects of excess lead iodide, Cs^+ , and Rb^+ on the phase composition of perovskite thin films.

RESULTS AND DISCUSSION

Incorporation of Cs^+ and Rb^+ into organic–inorganic hybrid lead iodide perovskite thin films has been shown to improve the film quality and phase purity of the desired cubic perovskite phase.^{10,16,17,22,23,27–29,32} To investigate the crystal structure of samples containing different cation compositions, two-dimensional reciprocal space maps were recorded, which are shown in Figure 1a–d. All films exhibit Bragg reflections of the cubic perovskite modification. The presence of additional features corresponding to hexagonal phases of FAPbI_3 and PbI_2 depends on the cation composition.

Azimuthal integration of the radially distributed intensity in the reciprocal space maps visualizes the relative total peak intensities (Figure 1e). In the double-cation compound, labeled as FA:MA , the intensity of the hexagonal phases 4H and 6H, occurring at small values of the scattering vector Q , is almost equal compared to the cubic phase. Also, in the corresponding reciprocal space map, the Bragg peaks from hexagonal phases and PbI_2 are clearly visible. The 4H and 6H hexagonal phases contain corner- and face-sharing lead halide octahedra and can be considered as intermediates between the 2H hexagonal δ -phase of FAPbI_3 , featuring only face-sharing octahedra, and the cubic perovskite phase comprising exclusively corner-sharing lead halide octahedra.³⁷

The sample containing excess PbI_2 exhibits stronger cubic phase peaks and less of the hexagonal phase but also a distinct amount of segregated lead iodide crystal phase, which is represented by the strong signal at $Q = 0.91 \text{ \AA}^{-1}$. However, the corresponding peak in the radial profile is rather broad and exhibits two additional shoulders due to an overlap with the signals from hexagonal phases, which are obviously still present in the material.

Addition of Cs^+ reduces both PbI_2 and hexagonal phase signals to a large degree, but small features of 4H and PbI_2 phases are still distinguishable at the corresponding positions of the green curve in Figure 1e and also in the reciprocal space map in Figure 1c. These are further diminished upon the incorporation of Rb^+ into the mixture, indicating a beneficial effect of using both inorganic cations. The quadruple-cation

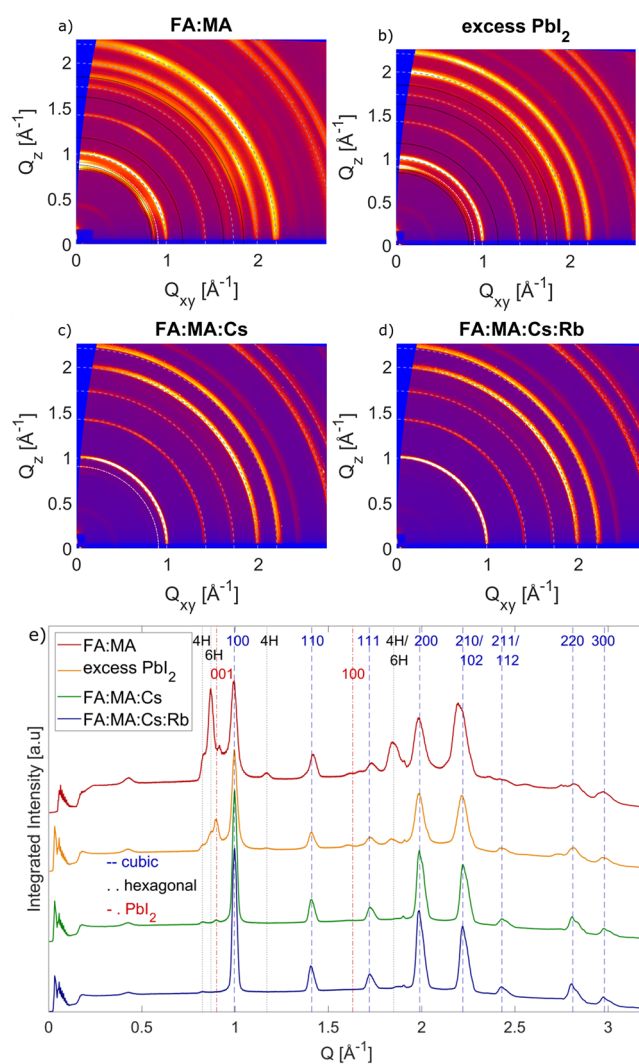


Figure 1. (a–d) 2D reciprocal space maps of samples with different compositions. Ring-shaped diffraction features indicate a random orientation of perovskite crystallites. Blue-dashed lines mark perovskite signals, hexagonal phases are labeled in black, and PbI_2 is denoted by pink lines. The incidence angle was 0.14° for measurement of all Q -maps. (e) Radial intensity distribution extracted from reciprocal space maps. Peaks are indexed according to the literature,³⁷ displaying a cubic perovskite crystal structure. Additional hexagonal and PbI_2 phases^{38,39} can be found for certain samples, as explained in the text.

composition almost exclusively displays the cubic perovskite modification, as can be seen in Figure 1d, where the distinct perovskite diffraction signals are marked. Nearly no residual hexagonal or PbI_2 phases can be found.

Quantification of the respective amounts of hexagonal and PbI_2 phases (Figure 2) was performed via integration of diffraction signals ascribed to the respective phases and using structure factor calculations, as described in the Experimental Section. We chose two different angles of incidence, 0.1° and 0.2° (Figure S2), to distinguish between surface and bulk properties. The incidence angle of 0.1° was determined to be just below the critical angle and is therefore supposed to reflect largely surface properties of the films. Increasing the incidence angle increases also the penetration depth of the X-rays into the material and is expected to reflect a larger amount of the

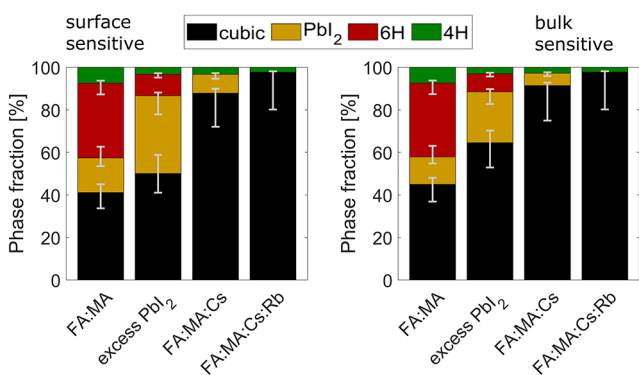


Figure 2. Molar phase fractions of cubic, hexagonal, and PbI_2 phases depending on the film composition, determined from peak integration of radial intensity profiles extracted from reciprocal space maps at incidence angles of 0.1° (left, surface-sensitive) and 0.2° (right, bulk-sensitive). Error bars were estimated due to compositional uncertainties and experimental statistics.

bulk film properties, which is therefore depicted by a 0.2° angle of incidence.

The trends in phase composition with varying cation mixtures are consistent for both incidence angles. FA:MA binary mixtures exhibit a huge amount of the 6H hexagonal polymorph, making up about 35% of the total investigated material volume, which is close to the content of the desired cubic phase. This could be extremely detrimental to the performance of the final device and might even be a potential trigger for further transition of the material to the photo-inactive δ -phase. Also, a significant contribution of the 4H polymorph and PbI_2 phase can be observed in the binary sample. Excess PbI_2 reduces the amount of hexagonal polymorphs significantly but occurs as a separate PbI_2 phase, which consequently can be observed in a higher fraction than in simple FA:MA mixtures. The quantity of the excess PbI_2 phase can be successfully reduced upon addition of Cs^+ and Rb^+ into the mixture, as can the appearance of hexagonal polymorphs. Solely adding Cs^+ , though reducing the intensities of impurity phases, still leaves residual PbI_2 and 4H phases in the films. The addition of both Cs^+ and Rb^+ , however, effectively suppresses the excess PbI_2 phase and 6H phase, while the 4H phase is reduced to a marginal amount of around 2% of the total material. This shows that even though the addition of Cs^+ has a beneficial effect on the phase composition of mixed perovskites, it is not sufficient to fully suppress impurity phases, especially that a considerable amount of excess PbI_2 is still present. An even higher phase purity can be obtained by adding both Cs^+ and Rb^+ to yield a quadruple-cation-mixed perovskite, almost exclusively (97.8%) consisting of the cubic perovskite modification. Cs^+ has been shown before to suppress the formation of hexagonal phases during the crystallization process,²³ while its effect on the excess lead iodide phase, even though it is reduced, does not suffice to prevent PbI_2 phase formation. On the contrary, Rb^+ has been reported to reduce PbI_2 phase impurities even under excess lead iodide conditions.²⁸ Hence, using both Cs^+ and Rb^+ has a joint effect and enables a high-purity cubic perovskite film.

Comparing the composition near the surface to the bulk material, a general trend of increasing proportions of hexagonal and PbI_2 phases as compared to the cubic perovskite phase with lowering the probing depth can be observed. Especially

for the excess lead iodide phase, this effect is strongly pronounced and suggests the location of PbI_2 preferably near the film surface. Decreasing intensities of the undesired phases with larger probing depth indicate that the bulk of the film contains less PbI_2 and hexagonal phases than areas near the surface, while for PbI_2 , the preference of surface areas seems the most pronounced and the fraction of hexagonal phases is only slightly lower in the bulk than near the surface, suggesting an almost equal distribution throughout the film. The prevalence of PbI_2 close to the surface might be due to an increased vulnerability of the perovskite surface toward degradation.

Improved purity of the perovskite phase upon inorganic cation addition is not only suggested by the disappearance of the peaks that were ascribed to impurity phases, i.e., lead iodide and hexagonal polymorphs. Also, a general peak sharpening can be observed, indicative of an improvement in crystal structure by enhanced crystallite size. Figure 3a shows

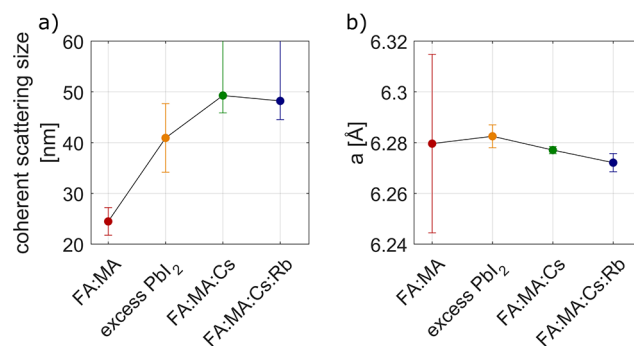


Figure 3. (a) Minimum coherently scattering island size as a function of composition, determined from Gaussian fits of peak widths (FWHM) of XRR data (Figure S1). Averaging was performed over different crystallographic directions, as similar trends could be observed for all of them. (b) Unit cell parameters as a function of composition, determined from Gaussian fits of peak positions observed in the XRR data.

sizes of homogeneous scattering domains determined from peak widths (FWHM) of X-ray reflectivity (XRR) data, averaged over different crystallographic directions. Consistent with the peak sharpening, which can be observed in the 2-dimensional Q -maps in Figure 1, calculations confirm an increase in crystallite size upon addition of excess lead iodide as well as inorganic cations. Here, adding Cs^+ had an even more enlarging effect than lead iodide, leading to an increase in crystallite size by at least a factor of two. However, the resolution limit of the experimental setup does not allow for the determination of coherently scattering island sizes larger than 50 nm, so the crystalline domains for the triple and quadruple-cation compositions might be even larger.

While on the incorporation of Cs^+ into the perovskite crystal lattice, a broad consensus is achieved,^{16,17,31,40–42} the question whether Rb^+ can also be integrated into the mixed perovskite crystal lattice is still discussed.^{27–29,32–34,40–43} To address this issue, lattice parameters of the cubic perovskite structure were determined for the different compositions. Figure 3b depicts the cubic unit cell parameter a as a function of composition. Data from XRR (Figure S1) was used to calculate the unit cell size from the positions of diffraction signals. From the calculated lattice parameters, it can be observed that excess PbI_2 leads to a small increase in the unit cell size compared to

the simple MA:FA mixture, which might be due to partial substitution of bromide ions in the mixture with the larger iodide ions.

Addition of Cs⁺ slightly shrinks the lattice, suggesting incorporation of the smaller inorganic cation in the hybrid perovskite, partially substituting for the larger organic cations FA⁺ and MA⁺ and thus decreasing the effective average cation radius.

Upon introduction of Rb⁺ into the material, a still smaller unit cell size is observed. Besides possible incorporation of the smaller Rb⁺ cation into the perovskite lattice, there might be several reasons for that. Rb⁺ has been found to interact strongly with iodide, leading to the formation of Rb- and I-rich side phases⁴⁴ and increasing the Br ratio in the perovskite phase, which also might cause a smaller lattice constant. Furthermore, since Cs⁺ has been observed to influence the distribution of Rb⁺ ions in the film,³³ the presence of Rb⁺ might reversely also alter the distribution of Cs⁺ in the material. The apparent lattice contraction upon Rb⁺ incorporation possibly could be also ascribed to those side effects and does not provide sufficient proof of incorporation of Rb⁺ into the perovskite lattice.

Detailed investigation of the azimuthally distributed intensity along the diffraction rings descending from the perovskite structure also revealed a small but still noticeable influence of cation composition on the orientational order of crystallites. An explicitly preferred orientation could be observed only for the (110) plane at an angle of 60° relative to the substrate (compare Figure S3). This finding is consistent with the previously reported orientation of the (202) plane parallel to the substrate.⁴⁵ However, the degree of orientational alignment is rather low in all samples, while it is strongest in the pure FA:MA mixture. Addition of excess PbI₂ or inorganic cations obviously affects the orientational alignment of crystallites and leads to randomization of orientation.

The impact of compositional engineering involving the incorporation of MA⁺, Cs⁺, and Rb⁺ cations and a mixture of them into the FAPbI₃ phase on the power conversion efficiencies (PCEs) of perovskite solar cells (PSCs) was evaluated under standard illumination conditions. For details, we refer to the Experimental Section.

As shown in Figure 4 and Table 1, a PSC containing a light absorption layer composed of FA_{1-x}MA_xPb(I_{3-x}Br_x) ($x \approx 17\%$) yielded a PCE of 12%, with a current density (J_{SC}) of 16.3 mA/cm², an open-circuit voltage (V_{OC}) of 1.042 V, and a fill factor (FF) of 68%. Adding an excess amount of PbI₂ to FA_{1-x}MA_xPb(I_{3-x}Br_x) increased the PCE to 18% (J_{SC} of 21.22 mA/cm², V_{OC} of 1.104 V, and FF of 75%), and by incorporating Cs⁺ into the FA_{1-x}MA_xPb(I_{3-x}Br_x) lattice, the PCE value was further improved to 20%. As summarized in Table 1, Cs⁺ incorporation improved the J_{SC} and V_{OC} , whereas the introduction of RbI into Cs-containing FA_{1-x}MA_xPb(I_{3-x}Br_x) precursor solution mainly increased the V_{OC} to 1.161 V, further supported by the average device metrics collected from a whole batch of samples presented in Figure S5. The trend exhibited by the J_{SC} values extracted from the J - V curves and hysteresis data (Table S6) is further substantiated by the corresponding incident photon-to-current conversion efficiency (IPCE) spectra (Figure 4b). Comparative analysis of the IPCE spectra illustrates that introduction of Cs⁺ increases the band gap with respect to the double-cation composition, whereas Rb⁺ incorporation in the precursor solution does not change the IPCE onset.⁴² Furthermore, the stabilized power

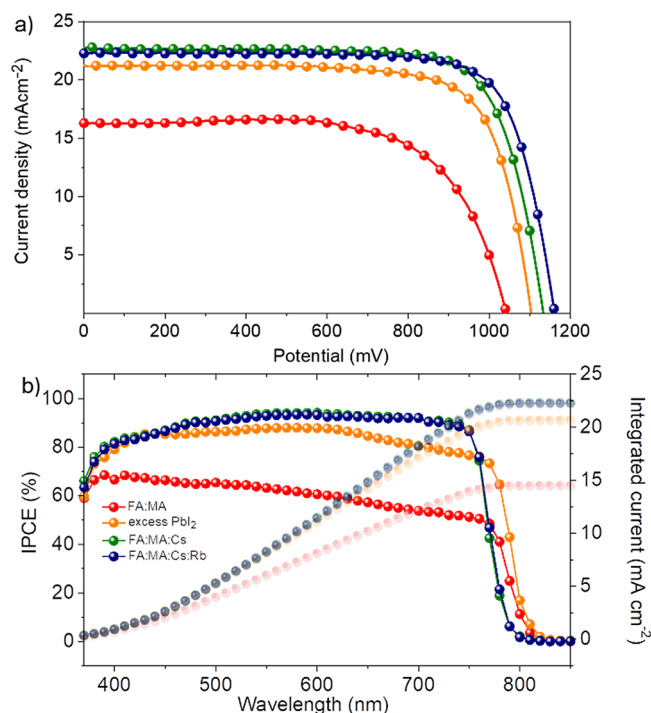


Figure 4. (a) Current density–voltage (J - V) characteristics measured under standard simulated AM1.5 illumination at a scan rate of 100 mV/s (reverse scan, with an illumination area of 0.16 cm²) corresponding to the devices based on the following architecture: FTO/c-TiO₂/m-TiO₂/Perovskite/Spiro/Au. (b) Incident photon-to-current conversion efficiency (IPCE) as a function of the monochromatic wavelength recorded for devices with different compositions and the integrated current density obtained from the respective IPCE spectrum.

Table 1. Photovoltaic Metrics Derived from the J - V Curve in Figure 4a

	V_{oc} (V)	J_{sc} (mA/cm ²)	FF (%)	PCE (%)
FA:MA	1.042	16.3	67.7	11.74
excess PbI ₂	1.104	21.22	75.3	18.0
FA:MA:Cs	1.134	22.72	76.0	20.1
FA:MA:Cs:Rb	1.161	22.28	76.8	20.24

output data (Figure S4) also coincided with the PCE values obtained through J - V measurements. Overall, the observed trend agrees with the literature.^{46,47}

Particularly, to understand the observed trend in the V_{oc} , we recorded steady-state and time-resolved photoluminescence (PL) (Figure 5). Steady-state PL (Figure 5a) revealed that excess PbI₂ does not influence the band gap of the double-cation perovskite, but with the introduction of Cs⁺, the band gap distinctly increases, while the introduction of Rb⁺ does not alter the band gap of the Cs-containing triple-cation-based perovskite. These findings are consistent with the IPCE data (Figure 4b).⁴² Time-resolved PL (Figure 5b) shows that the charge-carrier recombination slightly decreased when excess PbI₂ was used in the preparation. With the introduction of inorganic cations, the lifetime of the charge carriers increased further as τ_{10} (τ_{10} , when the PL intensity drops by an order of magnitude) increased from 430 ns to 600 and 770 ns, respectively, when Cs and (Cs + Rb) cations were introduced.⁴⁸ The presence of long-lived charge carriers infers the reduction in non-radiative recombination and the

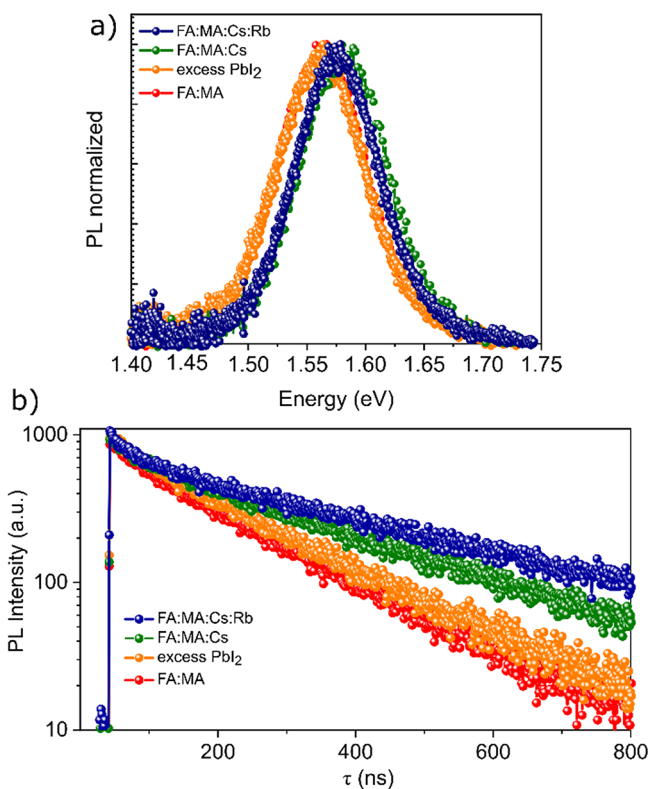


Figure 5. (a) Steady-state photoluminescence (PL) spectra showing widening of the band gap with the introduction of Cs cations and (b) time-resolved PL studies performed on samples with different compositions. The charge carrier lifetime improves in triple and quadruple-cation-based perovskite samples.

formation of high-quality perovskite films that enable the fabrication of PSCs yielding improved photovoltages, similar to previous reports.^{16,27}

CONCLUSIONS

In summary, a detailed investigation and quantification of the effects of mixing multiple cations in a hybrid lead halide perovskite including excess lead iodide conditions were conducted. The organic cations FA⁺ and MA⁺, as well as the inorganic cations Cs⁺ and Rb⁺, were used. Adding the smaller inorganic cations to yield triple- or quadruple-cation hybrid perovskites significantly improved the phase purity of the black photoactive cubic perovskite modification, enhancing its fraction from about 45% in the double-cation FA:MA mixture to 97.8% in the quadruple-cation material. Consequently, a reduction of hexagonal and PbI₂ phases in the perovskite thin films was observed. The quadruple mixture displayed the lowest amount of impurity phases, i.e., only about 2% of the 4H phase, indicating a beneficial effect of adding both Cs⁺ and Rb⁺. The phase composition also showed variations as a function of probing depth, such that especially PbI₂ was found preferentially near the film surface compared to the bulk of the film. Addition of excess PbI₂, as well as Cs⁺ and Rb⁺, also affected the crystal structure of the cubic perovskite, manifesting in a reduced amount of orientational order, a modification of lattice constants, and a significant increase in crystallite size. Finally, owing to improved phase purity of the photoactive layer, desired absorption and emission features were obtained, which led to the realization of photovoltaic

performance exceeding 20% from the PSCs employing triple- and quadruple-cation materials.

EXPERIMENTAL SECTION

Perovskite Film Preparation and Device Fabrication. The perovskite films were deposited using a single-step deposition method from the precursor solution containing FAI (1.0 M) (Greatcell Solar), PbI₂ (1.1 M) (TCI), MABr (0.2 M) (Greatcell Solar), and PbBr₂ (0.2 M) (TCI) in anhydrous dimethylformamide (99.8%, Acros)/dimethylsulfoxide (99.7%, Acros) (4:1 (v/v)). For the triple-cation composition, 5% CsI (1.5 M in DMSO, abcr GmbH, ultra-dry, 99.998%) was added to the precursor solution. To prepare the quadruple composition, 5% RbI (1.5 M in DMF/DMSO, 4:1 volume ratio, Sigma-Aldrich) was added to the triple-cation composition. The precursor solutions were spin-coated in a two-step program at 1000 and 6000 rpm for 10 and 30 s, respectively, onto the mesoporous TiO₂ films. During the second step, 100 μL of chlorobenzene (99.8%, Acros) was dropped on the spinning substrate 10 s prior to the end of the program. This was followed by annealing the films at 100 °C for 45 min. The substrates were cooled for a few minutes, and subsequently, a 200 nm-thick layer of spiro-OMeTAD (Merck) was spin-coated onto the perovskite layer, and the devices were completed by thermal evaporation of a 70–80-nm thick gold back contact layer under high vacuum. The deposition of perovskite and spiro-OMeTAD was carried out in a dry air glovebox under controlled atmospheric conditions with a humidity of <1%. The photovoltaic performance of the devices was evaluated under standard illumination conditions. All experimental procedures are reported elsewhere.^{16,27,34} Incident photon-to-charge carrier efficiency (IPCE) measurements were made using an LED light source (Ariadne EQE from Cici Research).

X-ray Diffraction Measurements. Experimental X-ray data was recorded at the ESRF beamline ID10 with photon energy $E = 22$ keV. To account for preferred orientation, typically observed for perovskite thin films, we used grazing incidence wide angle X-ray scattering (GIWAXS) to record reciprocal space maps³⁶ by employing a 2D Pilatus 300 K detector. All measurements were performed under a nitrogen atmosphere.

Determination of Relative Phase Fractions. To determine the fractions of different phases, intensities of the first Bragg peaks of each phase were used, located at $Q = 0.82 \text{ \AA}^{-1}$ for the 4H phase, $Q = 0.87 \text{ \AA}^{-1}$ for 6H, $Q = 0.91 \text{ \AA}^{-1}$ for PbI₂, and $Q = 0.99 \text{ \AA}^{-1}$ for the cubic phase. To normalize and compare the actual phase amounts, structure factor calculations were performed using the atomic positions in the crystal structures.^{37,38} In addition, the Lorentz correction and polarization correction were applied. Azimuthally integrated radial intensity profiles of reciprocal space maps at two different angles of incidence were used to distinguish bulk and surface composition, as described in the main text.

Photoluminescence Measurements. Photoluminescence and time-resolved photoluminescence spectra were recorded on a spectrofluorometer Fluorolog 322. Photoluminescence spectra were recorded by exciting the samples with a 450 W xenon lamp at a fixed wavelength of 450 nm and scanning the emission monochromator from 625 to 850 nm. The same spectrometer working in a time-correlated single-photon counting mode was used for time-resolved photoluminescence with sub-nanosecond time resolution. A picosecond pulsed diode laser head NanoLED-405LH (Horiba) emitting <200 ps duration pulses at 408 nm with a repetition rate of 1 MHz was used as an excitation source.

ASSOCIATED CONTENT

Supporting Information

The Supporting Information is available free of charge at <https://pubs.acs.org/doi/10.1021/acs.chemmater.0c04185>.

Additional photovoltaic and X-ray data (PDF)

■ AUTHOR INFORMATION

Corresponding Authors

Alexander Hinderhofer – Institute for Applied Physics,
University of Tübingen, 72076 Tübingen, Germany;
orcid.org/0000-0001-8152-6386;

Email: alexander.hinderhofer@uni-tuebingen.de

M. Ibrahim Dar – Cavendish Laboratory, Department of
Physics, University of Cambridge, Cambridge CB3 0HE,
United Kingdom; Laboratory of Photonics and Interfaces,
Department of Chemistry and Chemical Engineering, Ecole
Polytechnique Federale de Lausanne (EPFL), CH-1015
Lausanne, Switzerland; orcid.org/0000-0001-9489-
8365; Email: id3338@cam.ac.uk

Authors

Lena Merten – Institute for Applied Physics, University of
Tübingen, 72076 Tübingen, Germany

Thomas Baumeler – Laboratory of Photonics and Interfaces,
Department of Chemistry and Chemical Engineering, Ecole
Polytechnique Federale de Lausanne (EPFL), CH-1015
Lausanne, Switzerland

Neha Arora – Cavendish Laboratory, Department of Physics,
University of Cambridge, Cambridge CB3 0HE, United
Kingdom; orcid.org/0000-0003-4068-3574

Jan Hagenlocher – Institute for Applied Physics, University of
Tübingen, 72076 Tübingen, Germany

Shaik Mohammed Zakeeruddin – Laboratory of Photonics
and Interfaces, Department of Chemistry and Chemical
Engineering, Ecole Polytechnique Federale de Lausanne
(EPFL), CH-1015 Lausanne, Switzerland

Michael Grätzel – Laboratory of Photonics and Interfaces,
Department of Chemistry and Chemical Engineering, Ecole
Polytechnique Federale de Lausanne (EPFL), CH-1015
Lausanne, Switzerland; orcid.org/0000-0002-0068-0195

Frank Schreiber – Institute for Applied Physics, University of
Tübingen, 72076 Tübingen, Germany

Complete contact information is available at:

<https://pubs.acs.org/10.1021/acs.chemmater.0c04185>

Author Contributions

L.M., A.H., and F.S. wrote the manuscript with contributions from all authors. N.A., T.B., and M.I.D., with support of M.G., produced the samples and devices and acquired the results and with support of S.M.Z. and M.G. discussed the photovoltaic data. Photoluminescence measurements were performed by T.B. and were analyzed and discussed by T.B. and M.I.D. X-ray measurements were performed by A.H. and J.H., while data analysis was done by L.M. and A.H.

Notes

The authors declare no competing financial interest.

■ ACKNOWLEDGMENTS

The authors gratefully acknowledge funding by the DFG in the framework of the Priority Programme “Perovskite Semiconductors: From Fundamental Properties to Devices” (SPP 2196). We also thank the ESRF for granting synchrotron time and experimental assistance by Oleg Konovalov and Andrey Chumakov. M.I.D. acknowledges funding from a Royal Society University Research Fellowship. N.A. thanks the EPSRC project SUNRISE (EP/P032591/1). T.B. acknowledges support from the Swiss National Science Foundation (project no. IZJSZ2_180176).

■ ABBREVIATIONS

MA, methylammonium; FA, formamidinium

■ REFERENCES

- (1) Arora, N.; Dar, M. I.; Akin, S.; Uchida, R.; Baumeler, T.; Liu, Y.; Zakeeruddin, S. M.; Grätzel, M. Low-Cost and Highly Efficient Carbon-Based Perovskite Solar Cells Exhibiting Excellent Long-Term Operational and UV Stability. *Small* **2019**, *15*, 1904746.
- (2) Weber, D. CH₃NH₃PbX₃, ein Pb(II)-System mit kubischer Perovskitstruktur. *Z. Naturforsch.* **1978**, *33b*, 1443–1445.
- (3) Baikie, T.; Fang, Y.; Kadro, J. M.; Schreyer, M.; Wei, F.; Mhaisalkar, S. G.; Graetzel, M.; White, T. J. Synthesis and crystal chemistry of the hybrid perovskite (CH₃NH₃)PbI₃ for solid-state sensitised solar cell applications. *J. Mater. Chem. A* **2013**, *1*, 5628.
- (4) Eperon, G. E.; Stranks, S. D.; Menelaou, C.; Johnston, M. B.; Herz, L. M.; Snaith, H. J. Formamidinium lead trihalide: a broadly tunable perovskite for efficient planar heterojunction solar cells. *Energy Environ. Sci.* **2014**, *7*, 982.
- (5) Koh, T. M.; Fu, K.; Fang, Y.; Chen, S.; Sum, T. C.; Mathews, N.; Mhaisalkar, S. G.; Boix, P. P.; Baikie, T. Formamidinium-Containing Metal-Halide: An Alternative Material for Near-IR Absorption Perovskite Solar Cells. *J. Phys. Chem. C* **2014**, *118*, 16458–16462.
- (6) Conings, B.; Drijkoningen, J.; Gauquelin, N.; Babayigit, A.; D’Haen, J.; D’Olieslaeger, L.; Ethirajan, A.; Verbeeck, J.; Manca, J.; Mosconi, E.; Angelis, F. D.; Boyen, H.-G. ‘Intrinsic Thermal Instability of Methylammonium Lead Trihalide Perovskite’. *Adv. Energy Mater.* **2015**, *5*, 1500477.
- (7) Ke, J. C.-R.; Walton, A. S.; Lewis, D. J.; Tedstone, A.; O’Brien, P.; Thomas, A. G.; Flavell, W. R. In situ investigation of degradation at organometal halide perovskite surfaces by X-ray photoelectron spectroscopy at realistic water vapour pressure. *Chem. Commun.* **2017**, *53*, 5231.
- (8) Juarez-Perez, E. J.; Ono, L. K.; Maeda, M.; Jiang, Y.; Hawash, Z.; Qi, Y. Photodecomposition and thermal decomposition in methylammonium halide lead perovskites and inferred design principles to increase photovoltaic device stability. *J. Mater. Chem. A* **2018**, *6*, 9604.
- (9) Bryant, D.; Aristidou, N.; Pont, S.; Sanchez-Molina, I.; Chotchunangatchaval, T.; Wheeler, S.; Durrant, J. R.; Haque, S. A. Light and oxygen induced degradation limits the operational stability of methylammonium lead triiodide perovskite solar cells. *Energy Environ. Sci.* **2016**, *9*, 1655.
- (10) Turren-Cruz, S.-H.; Saliba, M.; Mayer, M. T.; Juárez-Santiesteban, H.; Mathew, X.; Nienhaus, L.; Tress, W.; Erodici, M. P.; Sher, M.-J.; Bawendi, M. G.; Grätzel, M.; Abate, A.; Hagfeldt, A.; Correa-Baena, J.-P. Enhanced charge carrier mobility and lifetime suppress hysteresis and improve efficiency in planar perovskite solar cells. *Energy Environ. Sci.* **2018**, *11*, 78.
- (11) Stoumpos, C. C.; Malliakas, C. D.; Kanatzidis, M. G. Semiconducting Tin and Lead Iodide Perovskites with Organic Cations: Phase Transitions, High Mobilities, and Near-Infrared Photoluminescent Properties. *Inorg. Chem.* **2013**, *52*, 9019.
- (12) Akin, S.; Arora, N.; Zakeeruddin, S. M.; Grätzel, M.; Friend, R. H.; Dar, M. I. New Strategies for Defect Passivation in High-Efficiency Perovskite Solar Cells. *Adv. Energy Mater.* **2020**, 1903090.
- (13) Jeon, N. J.; Noh, J. H.; Yang, W. S.; Kim, Y. C.; Ryu, S.; Seo, J.; Seok, S. I. Compositional engineering of perovskite materials for high-performance solar cells. *Nature* **2015**, *517*, 476.
- (14) Pellet, N.; Gao, P.; Gregori, G.; Yang, T.-Y.; Nazeeruddin, M. K.; Maier, J.; Grätzel, M. Mixed-Organic-Cation Perovskite Photovoltaics for Enhanced Solar-Light Harvesting. *Angew. Chem., Int. Ed.* **2014**, *53*, 3151.
- (15) Baumeler, T.; Arora, N.; Hinderhofer, A.; Akin, S.; Greco, A.; Abdi-Jalebi, M.; Shivanna, R.; Uchida, R.; Liu, Y.; Schreiber, F.; Zakeeruddin, S. M.; Friend, R. H.; Graetzel, M.; Dar, M. I. Minimizing the Trade-Off between Photocurrent and Photovoltage in Triple-Cation Mixed-Halide Perovskite Solar Cells. *J. Phys. Chem. Lett.* **2020**, *11*, 10188–10195.

- (16) Saliba, M.; Matsui, T.; Seo, J.-Y.; Domanski, K.; Correa-Baena, J.-P.; Nazeeruddin, M. K.; Zakeeruddin, S. M.; Tress, W.; Abate, A.; Hagfeldt, A.; Grätzel, M. Cesium-containing triple cation perovskite solar cells: improved stability, reproducibility and high efficiency. *Energy Environ. Sci.* **2016**, *9*, 1989.
- (17) Matsui, T.; Seo, J.-Y.; Saliba, M.; Zakeeruddin, S. M.; Grätzel, M. Room-Temperature Formation of Highly Crystalline Multication Perovskites for Efficient, Low-Cost Solar Cells. *Adv. Mater.* **2017**, *29*, 1606258.
- (18) Li, Z.; Yang, M.; Park, J.-S.; Wei, S.-H.; Berry, J. J.; Zhu, K. Stabilizing Perovskite Structures by Tuning Tolerance Factor: Formation of Formamidinium and Cesium Lead Iodide Solid-State Alloys. *Chem. Mater.* **2016**, *28*, 284.
- (19) McMeekin, D. P.; Sadoughi, G.; Rehman, W.; Eperon, G. E.; Saliba, M.; Horantner, M. T.; Haghighirad, A.; Sakai, N.; Korte, L.; Rech, B.; Johnston, M. B.; Herz, L. M.; Snaith, H. J. A mixed-cation lead mixed-halide perovskite absorber for tandem solar cells. *Science* **2016**, *351*, 151.
- (20) Yi, C.; Luo, J.; Meloni, S.; Boziki, A.; Ashari-Astani, N.; Grätzel, C.; Zakeeruddin, S. M.; Röthlisberger, U.; Grätzel, M. Entropic stabilization of mixed A-cation ABX₃metal halide perovskites for high performance perovskite solar cells. *Energy Environ. Sci.* **2016**, *9*, 656.
- (21) Shen, H.; Duong, T.; Peng, J.; Jacobs, D.; Wu, N.; Gong, J.; Wu, Y.; Karuturi, S. K.; Fu, X.; Weber, K.; Xiao, X.; White, T. P.; Catchpole, K. Mechanically-stacked perovskite/CIGS tandem solar cells with efficiency of 23.9% and reduced oxygen sensitivity. *Energy Environ. Sci.* **2018**, *11*, 394.
- (22) Tang, M.-C.; Fan, Y.; Barrit, D.; Li, R.; Dang, H. X.; Zhang, S.; Magnanelli, T. J.; Nguyen, N. V.; Heilweil, E. J.; Hacker, C. A.; Smilgies, D. M.; Zhao, K.; Amassian, A.; Anthopoulos, T. D. Efficient Hybrid Mixed-Ion Perovskite Photovoltaics: In Situ Diagnostics of the Roles of Cesium and Potassium Alkali Cation Addition. *Sol. RRL* **2020**, *4*, 2000272.
- (23) Dang, H. X.; Wang, K.; Ghasemi, M.; Tang, M.-C.; De Bastiani, M.; Aydin, E.; Dauzon, E.; Barrit, D.; Peng, J.; Smilgies, D.-M.; De Wolf, S.; Amassian, A. Multi-cation Synergy Suppresses Phase Segregation in Mixed-Halide Perovskites. *Joule* **2019**, *3*, 1746.
- (24) Bi, D.; Tress, W.; Dar, M. I.; Gao, P.; Luo, J.; Renievier, C.; Schenk, K.; Abate, A.; Giordano, F.; Baena, J.-P. C.; Decoppet, J.-D.; Zakeeruddin, S. M.; Nazeeruddin, M. K.; Grätzel, M.; Hagfeldt, A. Efficient luminescent solar cells based on tailored mixed-cation perovskites. *Sci. Adv.* **2016**, *2*, No. e1501170.
- (25) Seok, S. I.; Grätzel, M.; Park, N.-G. Methodologies toward Highly Efficient Perovskite Solar Cells. *Small* **2018**, *14*, 1704177.
- (26) Zhang, H.; Mao, J.; He, H.; Zhang, D.; Zhu, H. L.; Xie, F.; Wong, K. S.; Grätzel, M.; Choy, W. C. H. A Smooth CH₃NH₃PbI₃ Film via a New Approach for Forming the PbI₂ Nanostructure Together with Strategically High CH₃NH₃I Concentration for High Efficient Planar-Heterojunction Solar Cells. *Adv. Energy Mater.* **2015**, *5*, 1501354.
- (27) Saliba, M.; Matsui, T.; Domanski, K.; Seo, J.-Y.; Ummadisingu, A.; Zakeeruddin, S. M.; Correa-Baena, J.-P.; Tress, W. R.; Abate, A.; Hagfeldt, A.; Grätzel, M. Incorporation of rubidium cations into perovskite solar cells improves photovoltaic performance. *Science* **2016**, *354*, 206.
- (28) Duong, T.; Mulmudi, H. K.; Shen, H.; Wu, Y.; Barugkin, C.; Mayon, Y. O.; Nguyen, H. T.; Macdonald, D.; Peng, J.; Lockrey, M.; Li, W.; Cheng, Y.-B.; White, T. P.; Weber, K.; Catchpole, K. Structural engineering using rubidium iodide as a dopant under excess lead iodide conditions for high efficiency and stable perovskites. *Nano Energy* **2016**, *30*, 330.
- (29) Zhang, M.; Yun, J. S.; Ma, Q.; Zheng, J.; Lau, C. F. J.; Deng, X.; Kim, J.; Kim, D.; Seidel, J.; Green, M. A.; Huang, S.; Ho-Baillie, A. W. Y. High-Efficiency Rubidium-Incorporated Perovskite Solar Cells by Gas Quenching. *ACS Energy Lett.* **2017**, *2*, 438.
- (30) Park, Y. H.; Jeong, I.; Bae, S.; Son, H. J.; Lee, P.; Lee, J.; Lee, C.-H.; Ko, M. J. Inorganic Rubidium Cation as an Enhancer for Photovoltaic Performance and Moisture Stability of HC(NH₂)₂PbI₃ Perovskite Solar Cells. *Adv. Funct. Mater.* **2017**, *27*, 1605988.
- (31) Xu, Z.; Zhao, Y.; Zhang, J.; Chen, K.; Brabec, C. J.; Feng, Y. Phase diagram and stability of mixed-cation lead iodide perovskites: A theory and experiment combined study. *Phys. Rev. Mater.* **2020**, *4*, No. 095401.
- (32) Duong, T.; Wu, Y.; Shen, H.; Peng, J.; Fu, X.; Jacobs, D.; Wang, E.-C.; Kho, T. C.; Fong, K. C.; Stocks, M.; Franklin, E.; Blakers, A.; Zin, N.; McIntosh, K.; Li, W.; Cheng, Y.-B.; White, T. P.; Weber, K.; Catchpole, K. Rubidium Multication Perovskite with Optimized Bandgap for Perovskite-Silicon Tandem with over 26% Efficiency. *Adv. Energy Mater.* **2017**, *7*, 1700228.
- (33) Philippe, B.; Saliba, M.; Correa-Baena, J.-P.; Cappel, U. B.; Turren-Cruz, S.-H.; Grätzel, M.; Hagfeldt, A.; Rensmo, H. Chemical Distribution of Multiple Cation (Rb⁺, Cs⁺, MA⁺, and FA⁺) Perovskite Materials by Photoelectron Spectroscopy. *Chem. Mater.* **2017**, *29*, 3589.
- (34) Yadav, P.; Dar, M. I.; Arora, N.; Alharbi, E. A.; Giordano, F.; Zakeeruddin, S. M.; Grätzel, M. The Role of Rubidium in Multiple-Cation-Based High-Efficiency Perovskite Solar Cells. *Adv. Mater.* **2017**, *29*, 1701077.
- (35) Gao, B.; Meng, J. RbCs(MAFA)PbI₃ perovskite solar cell with 22.81% efficiency using the precise ions cascade regulation. *Appl. Surf. Sci.* **2020**, *530*, 147240.
- (36) Greco, A.; Hinderhofer, A.; Dar, M. I.; Arora, N.; Hagenlocher, J.; Chumakov, A.; Grätzel, M.; Schreiber, F. Kinetics of Ion-Exchange Reactions in Hybrid Organic-Inorganic Perovskite Thin Films Studied by In Situ Real-Time X-ray Scattering. *J. Phys. Chem. Lett.* **2018**, *9*, 6750.
- (37) Gratia, P.; Zimmermann, I.; Schouwink, P.; Yum, J.-H.; Audinot, J.-N.; Sivula, K.; Wirtz, T.; Nazeeruddin, M. K. The Many Faces of Mixed Ion Perovskites: Unraveling and Understanding the Crystallization Process. *ACS Energy Lett.* **2017**, *2*, 2686.
- (38) Mitchell, R. S. Structural polytypism of lead iodide and its relationship to screw dislocations. *Z. Kristallogr. Cryst. Mater.* **1959**, *111*, 372–384.
- (39) Ummadisingu, A.; Grätzel, M. Revealing the detailed path of sequential deposition for metal halide perovskite formation. *Sci. Adv.* **2018**, *4*, No. e1701402.
- (40) Kubicki, D. J.; Prochowicz, D.; Hofstetter, A.; Zakeeruddin, S. M.; Grätzel, M.; Emsley, L. Phase Segregation in Cs-, Rb- and K-Doped Mixed-Cation (MA)_x(FA)_{1-x}PbI₃ Hybrid Perovskites from Solid-State NMR. *J. Am. Chem. Soc.* **2017**, *139*, 14173.
- (41) Hu, Y.; Aygüler, M. F.; Petrus, M. L.; Bein, T.; Docampo, P. Impact of Rubidium and Cesium Cations on the Moisture Stability of Multiple-Cation Mixed-Halide Perovskites. *ACS Energy Lett.* **2017**, *2*, 2212–2218.
- (42) Uchida, R.; Binet, S.; Arora, N.; Jacopin, G.; Alotaibi, M. H.; Taubert, A.; Zakeeruddin, S. M.; Dar, M. I.; Grätzel, M. Insights about the Absence of Rb Cation from the 3D Perovskite Lattice: Effect on the Structural Morphological, and Photophysical Properties and Photovoltaic Performance. *Small* **2018**, *14*, 1802033.
- (43) Park, I. J.; Seo, S.; Park, M. A.; Lee, S.; Kim, D. H.; Zhu, K.; Shin, H.; Kim, J. Y. Effect of Rubidium Incorporation on the Structural, Electrical, and Photovoltaic Properties of Methylammonium Lead Iodide-Based Perovskite Solar Cells. *ACS Appl. Mater. Interfaces* **2017**, *9*, 41898.
- (44) Abdi-Jalebi, M.; Andaji-Garmaroudi, Z.; Pearson, A. J.; Divitini, G.; Cavocich, S.; Philippe, B.; Rensmo, H.; Ducati, C.; Friend, R. H.; Stranks, S. D. Potassium- and Rubidium-Passivated Alloyed Perovskite Films: Optoelectronic Properties and Moisture Stability. *ACS Energy Lett.* **2018**, *3*, 2671.
- (45) Dar, M. I.; Hinderhofer, A.; Jacopin, G.; Belova, V.; Arora, N.; Zakeeruddin, S. M.; Schreiber, F.; Grätzel, M. Function Follows Form: Correlation between the Growth and Local Emission of Perovskite Structures and the Performance of Solar Cells. *Adv. Funct. Mater.* **2017**, *27*, 1701433.
- (46) Arora, N.; Dar, M. I.; Hinderhofer, A.; Pellet, N.; Schreiber, F.; Zakeeruddin, S. M.; Grätzel, M. Perovskite solar cells with CuSCN hole extraction layers yield stabilized efficiencies greater than 20%. *Science* **2017**, *358*, 768.

(47) Abdi-Jalebi, M.; Dar, M. I.; Senanayak, S. P.; Sadhanala, A.; Andaji-Garmaroudi, Z.; Pazos-Outón, L. M.; Richter, J. M.; Pearson, A. J.; Sirringhaus, H.; Grätzel, M.; Friend, R. H. Charge extraction via graded doping of hole transport layers gives highly luminescent and stable metal halide perovskite devices. *Sci. Adv.* **2019**, *5*, No. eaav2012.

(48) Dar, M. I.; Jacopin, G.; Meloni, S.; Mattoni, A.; Arora, N.; Boziki, A.; Zakeeruddin, S. M.; Rothlisberger, U.; Grätzel, M. Origin of unusual bandgap shift and dual emission in organic-inorganic lead halide perovskites. *Sci. Adv.* **2016**, *2*, No. e1601156.